VOL. 20, NO. 20, OCTOBER 2025 ISSN 1819-6608
ARPN Journal of Engineering and Applied Sciences

www.arpnjournals.com

EFFECT OF NICKEL DOPING ON STRUCTURAL AND MAGNETIC PROPERTIES OF α-Fe_2O_3/TiO_2 NANOCOMPOSITES DERIVED FROM LOGAS NATURAL SAND FOR ENVIRONMENTAL APPLICATIONS

Erwin Amiruddin[1,4], Amir Awaluddin[2], Siti S. Siregar[2], Novalin Putri[3], Irene Yohanna[4] and Arif Haryadi[5]
[1]Department of Physics, Riau University, Pekanbaru, Indonesia
[2]Department of Chemistry, Riau University, Pekanbaru, Indonesia
[3]Civil Engineering Magister Study Program, Faculty of Civil Engineering, Laboratorium Jalan, Diponegoro University, Semarang, Central Java, Indonesia
[4]Ibnu Sina Islamic Hospital, Harjosari, Sukajadi, Pekanbaru, Indonesia
[5]Faculty of Cultural Sciences (FIB) University of North Sumatra, Indonesia
E-Mail: erwin.amiruddin@lecturer.unri.ac.id

ABSTRACT

In this study, α-Fe_2O_3/TiO_2 nanocomposites derived from Logas District natural sand as a raw material have been prepared by the ball milling method. The products of ball milling were doped with nickel nanoparticles at different doping concentrations (0, 1, 2, 3, and 4 wt. %). During the sample preparation, the impact of composition was studied using X-Ray Fluorescence (XRF) Spectroscopy. The effect of doping concentration on the structural and magnetic properties was studied using X-Ray Diffractometer (XRD) and vibration sample magnetometer (VSM), respectively. X-ray diffraction pattern confirmed the formation of α-Fe_2O_3/TiO_2 nanocomposites and a highly crystalline rhombohedral structure. The nickel doping did not change the structure of the nanocomposites; however, the average crystallite size decreases from 42.13 to 34.45 nm with increasing nickel doping concentration from 0 to 4 wt.%, respectively. The crystallite size based on the dominant peak (104) shows a similar trend as the nickel concentration increases. The magnetic properties of the samples show a ferromagnetic nature of the prepared nanocomposites. The saturation magnetization, remanence magnetization, and coercivity increase with increasing nickel concentration. This study demonstrates the simple way of preparing nickel-doped α-Fe_2O_3/TiO_2 nanocomposites for environmental applications.

Keywords: nanocomposites, ball milling, nickel-doped, titanium dioxide, logas natural sand.

Manuscript Received 22 September 2025; Revised 2 January 2026; Published 20 January 2026

INTRODUCTION

The increasing demand for sustainable and efficient materials in environmental remediation has driven extensive research into nanocomposites with tailored structural and magnetic properties. Among these, iron-based oxide nanomaterials, particularly hematite (α-Fe_2O_3), have received a lot of attention from researchers, not only in fundamental properties but also in their technological applications ranging from catalysts to biomedical applications [1, 2]. When combined with titanium dioxide (TiO_2), a well-known photocatalyst, these composites exhibit enhanced functionalities suitable for environmental applications such as pollutant degradation and water purification. The current applications of the nanocomposites, such as in environmental applications, require certain properties that can be achieved by controlling the preparation. Various techniques have been used to fabricate α- α-Fe2O3/TiO_2 nanocomposites of controllable morphology for various applications. There are several methods for preparing α- Fe_2O_3/TiO_2 nanocomposites, including sol gel [3,4], co-precipitation [5], solvothermal [6,7], hydrothermal [8], laser [9, 10], microwave-assisted[11], and ball milling [12, 13] methods. Among them, the ball milling method has been expected to be an effective strategies for used by many researchers [14] due to its high efficiency, simplicity, and low-cost mechanical technique for modifying the structure and morphology of nanocomposite materials uniformly and efficiently, and facilitating the doping of metals such as nickel into the oxide matrix. For example, previous researchers [15] used TiO_2/α-Fe_2O_3composite, which was prepared using the ball milling method, and applied it as a photocatalyst to degrade dyes like methylene blue with high degradation efficiency [16].

The degradation efficiency of α-Fe_2O_3/TiO_2 nanocomposites is still low since the band gap of α-Fe_2O_3 is wide (2.0-2.2 eV) [17], then its degradation efficiency and makes α-Fe_2O_3UV light responsive instead of visible light responsive. This is one of the weaknesses of α-Fe_2O_3/TiO_2 nanocomposites [13]. In order to overcome this weakness, doping α-Fe_2O_3/TiO_2 nanocomposites with transition metals, such as nickel, is one of the promising routes to intensify visible light receptive activity of Fe_2O_3/TiO_2 nanocomposites, therefore, can modify its optic and magnetic properties, potentially improving its catalytic activity[18]. Additionally, the utilization of natural resources, such as Logas natural sand from Riau Province, as raw materials offers an eco-friendly and economical approach to nanocomposite preparation, aligning with sustainable development goals.

To modify some specific properties, such as structural and magnetic properties ofα-Fe_2O_3/TiO_2 nanocomposites, wereport here the effect of nickel-doping on structural and magnetic properties of α-Fe_2O_3/TiO_2 nanocomposites derived from Logas natural sand using the ball milling method. Understanding these characteristics is crucial for optimizing their performance in environmental applications, including photocatalysis and magnetically recoverable systems. The integration of Logas' natural sand as a precursor not only underscores the potential for resource-efficient fabrication but also contributes to the advancement of environmentally benign nanomaterials for sustainable environmental management.

EXPERIMENTAL PROCEDURE

Raw Material and Chemical

The α-Fe_2O_3/TiO_2 nanocomposites in this study were prepared from Logas natural sand as a raw material. Nickel nanoparticles with a purity of 99.99% were purchased at Toko Pedia (www.tokopedia.com).

Preparation of Nickel Doped α-Fe_2O_3/TiO_2 Nanocomposites

Undoped and nickel-doped α-Fe_2O_3/TiO_2 nanocomposites were prepared using the ball milling method. At first, Logas sand samples were dried under the sun's rays until the samples were completely dried, and then processed using an iron sand separator (ISS) in order to roughly separate iron and non-iron oxide particles. The belt speed and sample vibration of ISS were 1.0 m/s and 2 Hz, respectively. The second step was to mill the ISS product using ball milling. The milling was carried out for 4 stages, in which each stage lasted for 50 hours. Each stage product of ball milling was processed using a strong NdFeB magnet for separating iron and non-iron oxide particles. Next, the product of the 4th stage ball milling was divided into 5 parts with the same amount of weight. Each part of the product was mixed with nickel nanoparticles at the concentrations of 0, 1, 2, 3, and 4 wt. % using ball milling for 20 hours, respectively.

Characterization Techniques

The composition, structural, and magnetic properties of the samples were characterized using X-Ray Fluorescence (XRF) Spectrometer, X-Ray Diffractometer (XRD), and Vibrating Sample Magnetometer (VSM), respectively. The XRD measurements were carried out using Cu-Kα radiation (1.5408 A˚). The scan range 2θ was from 10° to 100° at a scan speed of 5.0985°/min and step width of 0.01°. The magnetic properties of the samples were measured using VSM with an applied magnetic field ranging from -20.000Oe to 20.000Oe. For comparison, pure α-Fe_2O_3 nanoparticles were used.

RESULTS AND DISCUSSIONS

XRD Analysis

The effect of nickel doped on structural properties and crystallite size of α-Fe_2O_3/TiO_2 nanocomposites was studied by the X-ray diffraction (XRD) method. Figure-1 reveals the X-ray diffraction patterns of α-Fe_2O_3/TiO_2 nanocomposites prepared using the ball milling method. It is clear in the XRD patterns of the samples, all the sharp and single diffraction peaks of the XRD pattern of the sample confirm the formation of crystalline α-Fe_2O_3. In the as-prepared nanocomposites, α-Fe_2O_3 shows its characteristic peaks at (102), (104), (110), (113), (024), (116), (122), (214), (300), and (119) planes. Several peaks located at diffraction angles of 38.69°, 49.02°, and 56.72° appeared on the α-Fe_2O_3@TiO_2 nanocomposite samples are indexed to the phase of TiO_2 [19], which cannot be observed on Fe_2O_3 [20] as revealed in Figure-2. All diffraction peaks in the XRD pattern of prepared α-Fe_2O_3/TiO_2 nanocomposites were assigned to the Fe_2O_3 (JCPDS card No. 98-005-3677) and the TiO_2 (JCPDS card No. 98-006-2553) phases. In addition, pure α-Fe_2O_3 nanoparticles are used for comparison. The intensity of α-Fe_2O_3 peaks decreased after being combined with TiO_2 as compared to that of pure α-Fe_2O_3. This reduction is believed to be due to the effect of TiO_2 nanoparticles on α-Fe_2O_3 nanoparticles.

The intensity of the diffraction peaks decreases regularly with the increase of nickel concentration from 0 to 4 wt. %. This result confirms the successful doping of nickel into α-Fe_2O_3/TiO_2. The XRD patterns show an additional peak at a diffraction angle of 44.53° °, corresponding to the reflection plane of (111), which is characteristic of nickel (JCPDS file no. 04-850) [21]. The intensity of the reflection of the nickel phase increases as its content increases in α-Fe_2O_3/TiO_2 nanocomposites, which reveals the dominant presence of the nickel phase in the samples. No other impurity peaks are detected, indicating the higher phase purity of undoped and nickel-doped α-Fe_2O_3/TiO_2 nanocomposites, as indicated by the result of XRF measurement shown in Table-2, this result is in agreement with the results reported by Chinh *et al*. [22]. The diffraction patterns of α-Fe_2O_3/TiO_2 nanocomposites show that the nickel dopant alters the crystallinity but not the crystal structure of α-Fe_2O_3/TiO_2 nanocomposites. Therefore, the existence of diffraction peaks related to the nickel and α-Fe_2O_3/TiO_2 nanocomposites showed successful formation of α-Fe_2O_3/TiO_2-Ni nanocomposites using the ball milling method.

Additionally, the average crystallite sizes of the products were calculated with the Debye formula [23], $D=K\lambda/\beta Cos\theta$, where λ is the X-ray wavelength (around 0.154 nm), β is the width of the diffraction peak at its half maximum intensity (FWHM), and K is the shape factor (about 0.9), which are shown in Table-1. It is clear from Table-1 that a small shift of the diffraction peaks occurs in most peak positions to slightly lower angles. It can be noticed from Figure-3 that a small shift of the diffraction peaks occurs in most peak positions, with slightly lower

angles observed for nickel-dopedα-Fe_2O_3/TiO_2 nanocomposite. It is obvious that the grain sizes calculated based on the strongest peak 104 decrease with increasing nickel concentration. However, the grain sizes calculated based on all peaks on diffraction patterns vary with increasing nickel concentration of the samples. The calculated crystallite size was about 41.22 and 47.57 nm for α-Fe_2O_3 and α-Fe_2O_3/TiO_2 nanocomposites, respectively, which is slightly smaller than those found in our findings [24].

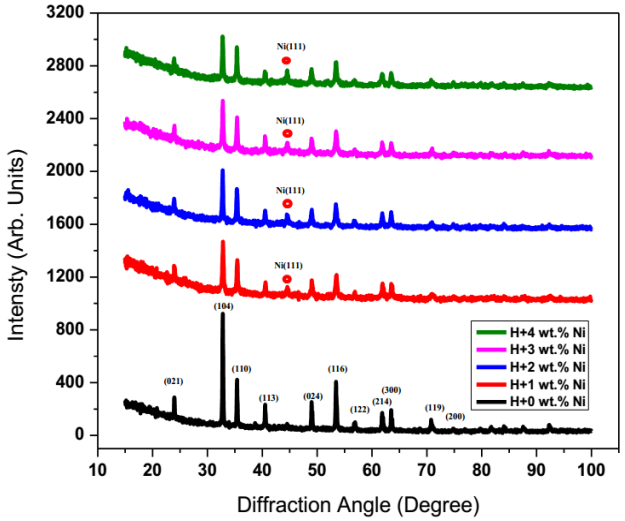

Figure-1. XRD patterns of nickel-doped α-Fe_2O_3/TiO_2nanocomposite with variation of nickel composition.

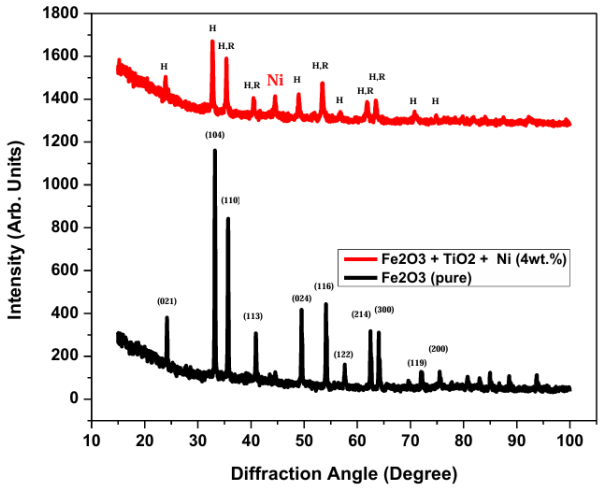

Figure-2. XRD patterns of pure hematite (black line) and 4 wt.% nickel-doped Fe_2O_3/TiO_2 nanocomposites (red line). The peaks are indexed with standard JCPDS cards, H-nickel-doped Fe_2O_3/TiO_2 nanocomposites, and R-TiO_2.

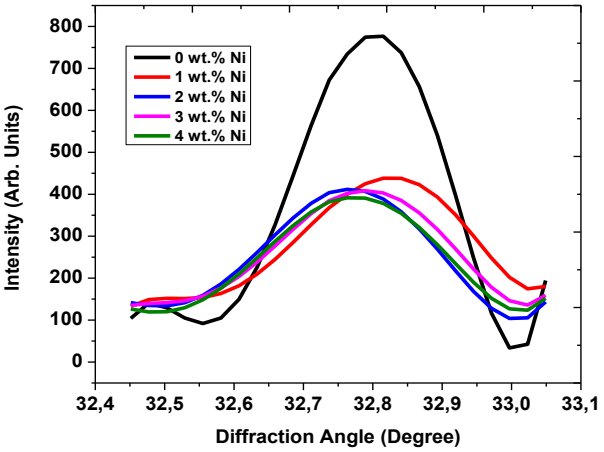

Figure-3. Expanded diffraction angle of 32.45.0º-33.05º showing shift of peak position to slightly lower angle.

Table-1. XRD pattern parameters for peak (104) of the nanocomposite.

Nickel Content (wt.%)	Intensity (Arb. Units)	2θ (Degree)	Crystallite Size (nm)	Average crystallite size (nm)
0	22	32.78	47.57	42.13
1	478	32.78	37.37	36.64
2	470	32.77	35.45	34.83
3	454	32.76	31.06	32.68
4	414	32.74	29.00	34.45

Concentration of the final product of ball milling after being milled for 200 hours and after being doped with 2 wt. % nickel was determined using X-Ray Fluorescence (XRF) Spectroscopy, presented in Table 2. It can be seen that the results clearly evidence the occurrence of iron oxide (α-Fe_2O_3), TiO_2 nanoparticles. The Table also indicates that the α-Fe_2O_3/ TiO_2 nanocomposites are not free from impurity elements such as silicon and other elements. The α-Fe_2O_3 and TiO_2 concentrations were decreased after being doped with 2 wt. % nickel. Some other compounds,

for example, SiO_2 decreased, and others were increased. This indicates that natural sand grains break into smaller parts so that the non-iron oxide and iron oxide were separated during the milling process.

Table-2. Compound composition of 2 wt. % nickel doped α-Fe_2O_3/TiO_2 nanocomposite after being milled for 200 hours observed by XRF.

Compound	Composition (%)	
	After milled 200 hours	After being doped 2 wt.% nickel
SiO_2	0.900	0.606
TiO_2	40.464	38.346
NiO	0.001	3.652
α-Fe_2O_3	53.274	51.862
Others	5.361	5.534

Magnetic Properties

The effect of nickel doped on the magnetic properties of α-Fe_2O_3/TiO_2 nanocomposites was analyzed Vibrating Sample magnetometer (VSM). The measurement was performed using an applied magnetic field sweeping from - 20 to +20 kOe. Figure-4 shows the magnetization versus applied magnetic field graph of the undoped nickel-doped α-Fe_2O_3/TiO_2 nanocomposites. All the hysteresis loops of the samples exhibited weak ferromagnetic behavior, which is in good agreement with those obtained in previous observations [24]. The magnetic parameters consisting of saturation magnetization (Ms), remanence magnetization (Mr), and coercivity (Hc) of the as-prepared undoped and nickel-doped Fe_2O_3/TiO_2 nanocomposite are summarized in Table-3. The Ms, Mr, and Hc values of the samples increase as the nickel concentration increases. The increase in the saturation magnetization might be because nickel is a magnetic nanoparticle, which then leads to the higher magnetic moment per unit mass.

The undoped Fe_2O_3/TiO_2 nanocomposite has a coercivity of about 170 Oe. The hysteresis loop of this sample shows superparamagnetic behavior with which higher value of magnetization and a smaller value of coercivity. In comparison, the saturation magnetization value of nickel-doped Fe_2O_3/TiO_2 nanocomposite is higher than that of the pure hematite nanoparticles, as presented in Figure-5. This is due to several factors, such as size, crystalline and crystal defect [25], and the purity of the prepared samples. The coercivity of undoped α-Fe_2O_3/TiO_2 nano composites increases to 275, 280, 282, and 285 Oe with nickel concentration of 1, 2, 3, and 4 wt.% %, respectively as indicated in Table-3. Thus, the increase of coercivity in this range of nickel concentration can be qualitatively understood in terms of the effect of relatively loosely coupled iron oxide nanoparticles, followed by the increase in iron oxide nanoparticles separation, which ultimately reduces exchange increase between weakly coupled iron oxide nanoparticles or clusters [26]. The smaller coercivity for nickel-doped samples compared to that of our previous finding [27] can be attributed to the difference in morphological properties and reduced magneto-crystalline anisotropy.

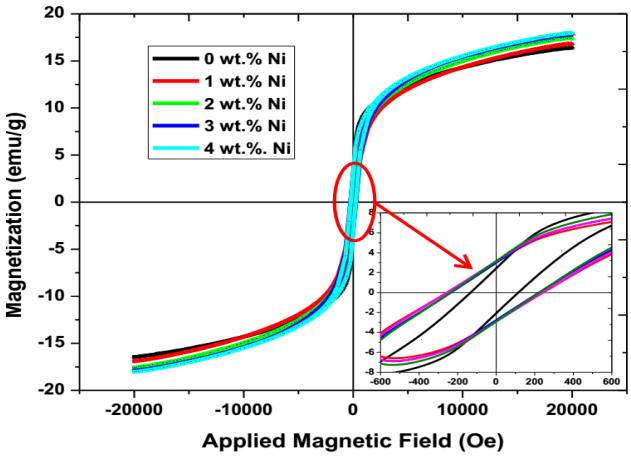

Figure-4. Hysteresis loops of nickel-doped α-Fe_2O_3/TiO_2 nanocomposite with different nickel concentrations (wt. %).

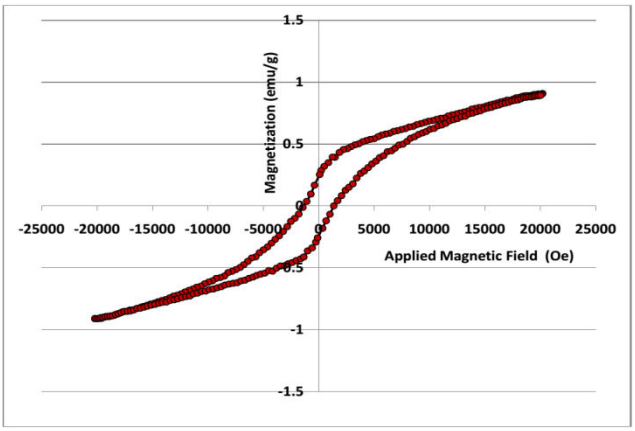

Figure-5. Hysteresis loop of pure hematite (α-Fe_2O_3).

Table-3. Hysteresis loop parameters of undoped and nickel-doped α-Fe_2O_3/TiO_2 nanocomposite.

Nickel content (wt.%)	Ms (emu/g)	Mr (emu/g)	Hc (Oe)	Mr/Ms
0	16.4223	2.5	170	0.152
1	16.8324	3.3	275	0.196
2	17.4325	3.5	280	0.201
3	17.8326	3.4	282	0.191
4	18.0123	3.5	285	0.194

CONCLUSIONS

The undoped and nickel-doped α-Fe_2O_3/TiO_2 nanocomposite with different nickel concentrations (0, 1, 2, 3, and 4 wt.%) based on Logas natural sand was successfully prepared by the ball milling method. Structural studies revealed that the samples are crystallized in a single-phase rhombohedral crystal structure of α-Fe_2O_3. The average crystallite size of the samples decreases as nickel concentration increases. When the nickel concentration increases from 0 to 4 wt. %, a nickel peak (111) was detected by XRD. The intensity of this (111) peak increases with increasing nickel concentration. The existence of diffraction peaks related to the nickel and α-Fe_2O_3/TiO_2 nanocomposite showed a successful ball milling method to form α-Fe_2O_3/TiO_2-Ni nanocomposite. The magnetic studies confirm the ferromagnetic nature of the samples. The saturation magnetization (Ms), remanent magnetization (Mr), and coercivity (Hc) of α-Fe_2O_3/TiO_2–Ni nanocomposite increase with increasing nickel concentration. This result indicated that the obtained undoped and nickel-doped α-Fe_2O_3/TiO_2 nanocomposite prepared by the ball milling method is a potential material for environmental applications.

ACKNOWLEDGMENTS

This work was financially supported by the Directorate of Research and Community Service (DPPM) through the Directorate General of Research and Development (Ditjen Risbang), Ministry of Higher Education, Science, and Technology, Republic of Indonesia 2025. The authors are grateful to the National Research and Innovation Agency (BRIN) Indonesia for conducting the VSM measurements, the Physics department UNP Padang for XRD measurements, magnetic research group members in the Magnetic Laboratory FMIPA UNRI for their assistance during sample collection and preparation.

REFERENCES

[1] Padmanabhan N. T., Thomas N., Louis J., Methew D. T., Ganguly P., Pillai S. C. 2021. Graphene-coupled TiO_2 Photocatalysts for environmental applications. A review. Chemosphere. 271: 129506.

[2] Akbarzadeh A., Samiei M., Davaran S. 2012. Magnetic properties, nanoparticles: preparation, physical, and applications in biomedicine. Nanoscale Res. Lett. 7: 144.

[3] Reda M. Mohamed, Mohammad W. Kadi, Adel A. Ismail. 2020. A Facile synthesis of mesoporous α-Fe_2O_3/TiO_2 nanocomposites for hydrogen evolution under visible light. Ceramics International.46: 10A, 15604-15612.

[4] Magesan Paramanandham. 2020. X-ray diffraction and morphological studies of Fe_2O_3-doped TiO_2 nanocomposites. Malaya Journal of Matematik, S: 2, 2163-2166.

[5] Houda Mansour, K. Omri, Radhouane Bargougui, Salah Ammar. 2020.Novel α-Fe_2O_3/TiO_2 nanocomposites with enhanced photocatalytic activity. Applied Physics A. 126: 151.

[6] Ying Yang, Qian Zhang, Yuhang Deng, Chuanda Zhu, Di Wang, Zhenquan Li. 2017. Synthesis of Nano TiO_2-Fe_2O_3 Photocatalyst and photocatalytic degradation properties on oxytetracycline hydrochloride. Advances in Engineering Research. 128: 216-219.

[7] Zhu D., Zhang J., Song J., Wang H., Yu Z., Shen Y., Xie A. 2013. Efficient one-pot synthesis of hierarchical flower-like α- Fe_2O_3 hollow spheres with excellent adsorption performance for water treatment. Appl Surf Sci. 284: 855-61.

[8] Das S., Saha S. K. 2017. Hydrothermal synthesis of Fe_2O_3/TiO_2 nanocomposites for dye degradation. Materials Science in Semiconductor Processing. 65: 99-106.

[9] Suiyuan Chen, Y.-K. Zhang, D. Wellburn, C.-S. Liu. 2013. Synthesis of Fe_2O_3-TiO_2 nanocomposite particles by pulsed laser control. Journal of Northeastern University. 34(2): 205-208

[10] Suiyuan Chen, Yikun Zhang, Weili Han, Daniel Wellburn, Jing Liang, Changsheng Liu. 2013. Synthesis and magnetic properties of Fe_2O_3- TiO_2 nano-composite particles using pulsed laser gas phase evaporation-liquid phase collecting method. Applied Surface Science. 283: 422-429.

[11] Abdullah Al Nahid. 2024. Microwave-assisted sol-gel synthesis of Fe_2O_3-@TiO_2 core-shell nanocomposite for the enhanced photocatalytic activity under visible light and the investigation of their optical properties. Advanced Powder Technology. 35(12): 104714.

[12] Tanmay K. Ghoraia, Mukut Chakrabortya, Panchanan Pramanik. 2011. Photocatalytic performance of nano-photocatalyst from $TiO_2$and Fe_2O_3 by mechanochemical synthesis.Journal of Alloys and Compounds. 509: 8158-8164.

[13] Erwin Amiruddin, Salomo Sinuraya, Amir Awaluddin, Martha Rianna, Heri Hadianto, Muhammad Rizki, Novia Magdalena Purba, and Indah Tamara Sitorus. 2023. Chromium Doped Iron Oxide Nanoparticles and Physical Properties Prepared from Logas Natural Sand and Their Application in Photo-Fenton Degradation of Methylene Blue Dye. ARPN Journal of Engineering and Applied Sciences. 18(10): 1102-1110.

[14] Mercyrani Babudurai, Onyekachi Nwakanma, Araceli Romero- Nuñez, Ravichandran Manisekaran, Velumani Subramaniam, Homero Castaneda, Anish Jantrania. 2021. Mechanical activation of TiO2/Fe_2O_3- nanocomposite for arsenic adsorption: effect of ball-to-powder ratio and milling time. Journal of Nanostructure in Chemistry. https://doi.org/10.1007/s40097-021-00388-8

[15] S. Lubis, I. Maulana, and M. 2018. Synthesis and Characterization of TiO2/α-Fe_2O_3 Composite using Hematite from Iron Sand for Photodegradation Removal of Dye. J. Nat. 18: 1, 38-43.

[16] S. C. Lee, H. O. Lintang, and L. Yuliati. 2017. High photocatalytic activity of Fe_2O_3/TiO_2 nanocomposites prepared by photodeposition degradation of 2, 4-dichlorophenoxyacetic acid. Beilstein J. Nanotechnol. 8: 1, 915-926.

[17] Gilbert B., Frandsen C., Maxey er, Sherman D. M. 2009. Band-gap measurements of bulk and nanoscale hematite by soft X-ray spectroscopy. Phys Rev B. 79: 35108-1-35108-7.

[18] Teguh P. Hadilala, Erwin Amiruddin1, Amir Awaluddin, Rahmondia Nanda Setiadi. 2024. Preparation and characterization of Cr-TiO_2/α-Fe_2O_3 nanocomposite for methylene blue degradation. Indonesian Physics Communication. 21: 3, 205-210

[19] Houda Mansour, K. Omri, Radhouane Bargougui, Salah Ammar. 2020. Novel α-Fe2O3/TiO2 nanocomposites with enhanced photocatalytic activity, Applied Physics A. 126:151. doi.org/10.1007/s00339-020-3320-3

[20] Erwin Amiruddin, Amir Awaluddin, Ari Sulistyo Rini, Dewi Natalia Hutahuruk, Miftahul Jannah and Novalin Putri. 2024. Structural and magnetic properties of α-Fe_2O_3/TiO_2 nanocomposite derived from Logas natural sand for environmental application. ARPN Journal of Engineering and Applied Sciences. 19: 23, 1409-1415.

[21] M. Saitou. 2016. Internal Stress in Nickel Thin Films Affected by Additives in Electrodeposition. International Journal of Electrochemical Science. 11: 2, 1651-1660

[22] Chinh Van Tran, Phuong T. H. Nguyen, Duy Anh Nguyen, Bac Thanh Le, Tuan Ngoc Truong, Duong Duc La. 2018. Facile fabrication and characterization of nanostructured Fe2O3-TiO2 composite from Ilmenite ore. International Journal of Advanced Engineering, Management and Science (IJAEMS). 4: 7, 574-578.

[23] B. D. Cullity, S. R. Stock, Elements of X-ray Diffraction in Diffraction III: Real Samples, 3rd edn. 170 (Addison-Wesley, Boston, Chap. 5, 1978).

[24] Erwin Amiruddin, Amir Awaluddin, Martha Rianna, Miftahul Haqie Al Firdaus, Syavia Rofiqa, Sella Audina Putri and Artika Dewi Sitangang. 2023. Structural, magnetic, and optical properties of nickel-doped iron oxide nanoparticles based on Logas natural sand for environmental application. ARPN Journal of Engineering and Applied Sciences. 18: 17, 1984-1990.

[25] X. L. Xie, H. Q. Yang, F. H. Zhang, L. Li, J. H. Ma, H. Jiao, J. Y. Zhang. 2009. J. Alloys Compd. 477: 90-99

[26] Erwin and Adhy Pryayitno. 2017. Magnetic exchange interaction in cobalt samarium thin films for high-density recording media. ARPN Journal of Engineering and Applied Sciences. 12: 12, 3832-3835.

[27] Erwin Amiruddin, Salomo Sinuraya, Rahmondia N. Septiadi, Yanuar Hamzah, Amir Awaluddin, Loly A. Hardani, Fitri A. Lestari, Yessi Magdalena, and Devi T. Gurning. 2022. A Systematic Study of the Structural and Magnetic Properties of Nickel Doped α-Fe_2O_3 nanoparticles Prepared from Logas Natural Sand. ARPN Journal of Engineering and Applied Sciences. 17(14): 1408-1413.